Eur. Phys. J. Plus (2023) 138:761
https://doi.org/10.1140/epjp/s13360-023-04398-z

THE EUROPEAN PHYSICAL JOURNAL PLUS

Regular Article

Detecting properties of echoes from the inspiraling stage with ground-based detectors

Xing-Yu Zhong[1,2,5,a], **Wen-Biao Han**[3,1,2,4,b], **Ye Jiang**[1], **Ping Shen**[1], **Shu-Cheng Yang**[1], **Chen Zhang**[1]

[1] Shanghai Astronomical Observatory, Chinese Academy of Sciences, Shanghai 200030, China
[2] School of Astronomy and Space Science, University of Chinese Academy of Sciences, Beijing 100049, China
[3] School of Fundamental Physics and Mathematical Sciences, Hangzhou Institute for Advanced Study, UCAS, Hangzhou 310024, China
[4] Taiji Laboratory for Gravitational Wave Universe (Beijing/Hangzhou), University of Chinese Academy of Sciences, Beijing 100049, China
[5] OzGrav-ANU, Centre for Gravitational Astrophysics, College of Science, The Australian National University, ACT 2601, Australia

Received: 19 February 2023 / Accepted: 18 August 2023

Abstract The nature of black holes is one of the most exciting issues in gravitational physics. If there is an exotic compact object as compact as a black hole but without a horizon, gravitational wave echoes may be produced after the merger. In this work, we show that for extreme-mass-ratio binaries, even during the inspiraling phase of compact binary coalescence, the existence of the hard surface of the exotic compact object will produce detectable signals on the gravitational waves. We predict that once the LIGO-Virgo-KAGRA, Einstein Telescope, or Cosmic Explorer detect such kinds of sources, our model shows that one can constrain the properties of surfaces of the compact objects in inspiraling stage better than the current level.

1 Introduction

The updated gravitational wave (GW) catalog shows that more than 90 GW events have been detected by LIGO-Virgo-KAGRA (LVK). Most of these events are inferred as binary black holes or black hole—neutron star mergers [1]. These observations give us a unique opportunity to test the nature of black holes, especially the horizon which is a key task in GW astronomy [2, 3].

Exotic compact objects (ECOs) are black hole-like but horizonless compact objects other than neutron stars. The candidates of ECOs could be abundant, such as fluid star, gravastar, bubble, fuzzball, and superspinars [4, 5]. These ECOs are black holes-like but without horizons, replaced by surfaces very close to the horizons of the corresponding black holes. The surface locates at the Planck scale outside of the horizon, and new physics may hide. The radius of surface of ECO is $r_0 = (1+\epsilon)(M+\sqrt{M^2-a^2})$, where a is the Kerr parameter. While $\epsilon = 0$, we go back to a black hole. For neutron stars, $\epsilon \sim \mathcal{O}(1)$. For ECOs, we expect that $r_0 - r_\mathrm{h}$ is of the order of the Planck length l_P, in such case $\epsilon \sim 10^{-40}$ or even smaller. Assuming $\epsilon \ll 1$, one can test the BH paradigm in an agnostic way, or for testing the effects of quantum gravity [5].

For black holes, the effective potential will reduce to zero after the light ring. However, for a horizonless compact object, due to the hard surface, there are potential well supports for quasi-trapped, long-lived modes, which are called gravitational wave echoes [6]. Theoretically, people discussed the physical mechanism of echoes from ECOs [7–9]. Some of us calculated echoes from Kerr-like ECOs using the Teukolsky equation with reflecting boundary [10]. A few pieces of literature have tried to find echoes from the LIGO data and give the parameter estimations on ECOs [11–15].

All these attempts are searching the echoes directly after ringdown to constrain the existence of ECOs. From Fig. 1, one can see that the echo signal is much weaker than the inspiral-merger-ringdown one. Therefore, it is difficult to constrain or detect echoes. However, due to the reflection property of the surface of ECO, the energy flux of gravitational radiation involving an ECO is different from the case of a black hole. This will induce a dephasing of GWs during the inspiral stage and potentially can be detected. Naively, we can expect that a longer inspiral signal makes distinguishing between a black hole and an ECO easier. The long inspiral asks for a large mass ratio ν. Datta et al. [16] considered this effect of the extreme-mass-ratio inspirals (EMRIs) and concluded that it could be detected by EMRIs, i.e., using space detectors. In the present work, we investigate the extreme-mass-ratio binaries (EMRBs) which are composed of a light black hole (a few solar masses), a neutron star (NS), or even a primordial black hole (PBH), and a much massive black hole (MBH, from a few tens to more than 100 solar masses), and it can be used to detect this effect by LVK events. The LVK has already detected events with a mass ratio of 1:26 (GW191219_163120 [17]), and O4 maybe detect more EMRBs with larger mass ratios.

[a] e-mail: zxy@shao.ac.cn
[b] e-mail: wbhan@shao.ac.cn (corresponding author)

Published online: 27 August 2023

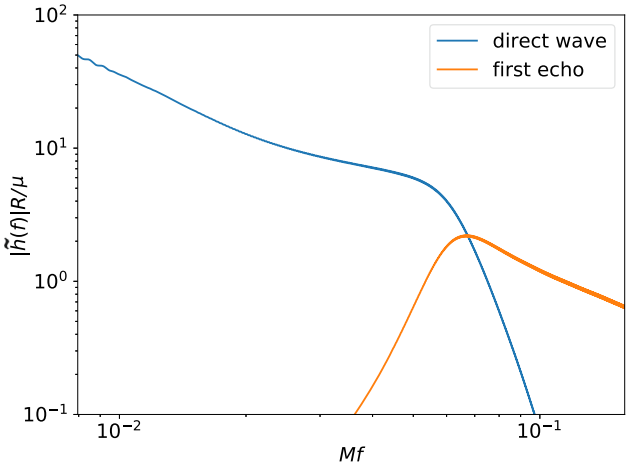

Fig. 1 The scaled amplitudes (μ is the reduced mass of the system and R is the distance) of the frequency domain signals $\tilde{h}(f)$. The blue solid line is the inspiral waveform and the orange solid line is the echo

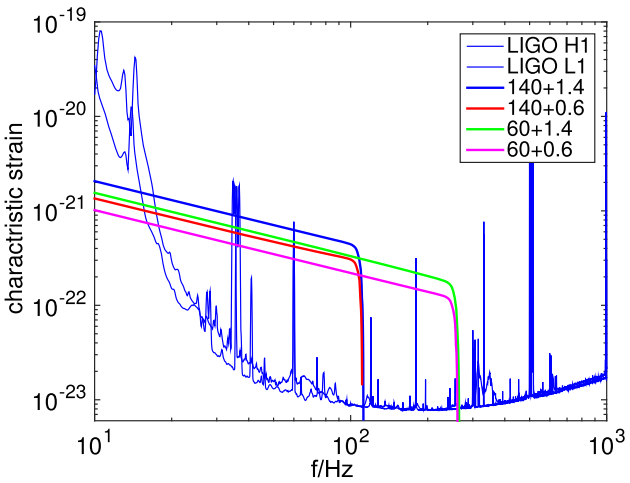

Fig. 2 Characteristic strains of four EMRBs composed by massive black holes (140 or 60 solar masses) and neutron stars (1.4 $M_\odot$) or primordial black holes (0.6 $M_\odot$), the sources are located at 100 Mpc from the Earth. The PSDs of the GW150914 event here are only for demonstration purposes, and the PSDs used for all the analytical calculations in this paper are the updated advanced LIGO sensitivity design curve LIGO-T180004

We will see that for the EMRB with a mass ratio of 60:1, the influence of the quantum surface of ECO on the energy flux will induce detectable dephasing on the inspiral signal. LVK has found several events with an obvious asymmetric mass ratio. GW190814 has two components with 23 and 2.6 solar masses; GW200210_092254 is composed of 24 and 2.8 solar mass objects. Especially, GW191219_163120 has the largest mass-ratio until now, 31: 1.2. In the coming O4 run of LIGO-Virgo-KAGRA, it is possible to detect more large mass-ratio binaries, i.e., EMRBs.

Up to now, LIGO-Virgo has detected the most massive black hole with 107 $M_\odot$ before the merger and the final mass of the remnant black hole at 174 $M_\odot$ in GW170426_190642 event [1]. The lightest compact object (neutron star) is 1.2 $M_\odot$ in GW191219_163210. It is worth expect LIGO-Virgo-KAGRA will detect extreme-mass-ratio binaries composed of a very heavy black hole and a light compact object with a mass ratio typically larger than 20 in the future. This kind of source has enough signal-to-noise ratio (SNR) for detections (Fig. 2), even the second small objects are neutron stars (NSs) with 1.4 $M_\odot$ or primordial black holes (PBHs) with only 0.6 solar mass. In this work, we use 4 EMRBs: NS (1.4 solar mass) + 140 solar mass MBH/ECO (Sys 1), PBH (0.6 solar mass) + 140 solar mass MBH/ECO (Sys 2), neutron star + 60 solar mass MBH/ECO (Sys 3), and PBH + 60 solar mass MBH/ECO (Sys 4) to demonstrate the potential capability of LIGO-Virgo constraint on the ECOs. For calculating the gravitational waves from the small compact objects inspiraling into the massive BHs or ECOs, especially the effects due to the hard surface of ECOs, we employ the Teukolsky equation [18] to fulfill this task by introducing "reflectivity" of the ECO surface. Distinguishing from the previous works of searching the direct echoes (i.e., the orange line in Fig. 1)after ringdown signals, we focus on the influence of the surface on the inspiraling part before the plunge (i.e., the blue line in Fig. 1). Note that all the waveforms we show are calculated based on the Teukolsky equation with the spin weight $s = -2$.

This paper is organized as follows. In the next section, we introduce our numerical method for calculating the waveforms. The energy flux and the result will be described in Sect. 4. Finally, we will conclude.

2 Waveforms and orbital evolution

By using effective-one-body (EOB) dynamics and black hole perturbation theory, gravitational radiations from EMRBs have been investigated for Schwarzschild in [19] and Kerr MBHs [20]. Later, the so-called ET codes of [20] were developed to use the Teukolsky-based fluxes to source the EOB dynamics. Here, we use "ET" codes to calculate the waveforms. In the Teukolsky equation, decomposing the Weyl curvature component ψ_4 in a Fourier transformation:

$$\psi_4 = \frac{1}{(r - ia\cos\theta)^4}\int_{-\infty}^{+\infty} d\omega \sum_{lm} R_{lm\omega}(r)\ {}_{-2}S_{lm}^{a\omega}(\theta)e^{-i\omega t+im\phi} \tag{1}$$

with the radial function $R_{lm\omega}$ and the spin-weighted spheroidal harmonics ${}_{-2}S_{lm}^{a\omega}$, the radial master equation of the Teukolsky equation is

$$\Delta^2\frac{d}{dr}\left(\frac{1}{\Delta}\frac{dR_{lm\omega}}{dr}\right) - V(r)R_{lm\omega} = -\mathcal{T}_{lm\omega}(r), \tag{2}$$

where $\Delta = r^2 - 2Mr + a^2$, $R_{lm\omega}$ is the radial function, $\mathcal{T}_{lm\omega}(r)$ is the source term, which is decided by the energy-momentum tensor of the perturber, and $V(r)$ is potential.

We use Green's function theory to obtain a general solution to the Teukolsky equation [22], which first requires solving its homogeneous equation. The homogeneous solution has two types of asymptotic behaviors which are purely incoming at the horizon and purely outgoing at infinity:

$$R^H_{lm\omega} = B^{\rm hole}_{lm\omega}\Delta^2 e^{-ip_{m\omega}r^*}, r\to r_+;\quad R^H_{lm\omega} = r^3 B^{\rm out}_{lm\omega}e^{i\omega r^*} + r^{-1}B^{\rm in}_{lm\omega}e^{-i\omega r^*}, r\to\infty \tag{3}$$

and

$$R^\infty_{lm\omega} = D^{\rm out}_{lm\omega}e^{ip_{m\omega}r^*} + \Delta^2 D^{\rm in}_{lm\omega}e^{-ip_{m\omega}r^*}, r\to r_+;\quad R^\infty_{lm\omega} = r^3 D^\infty_{lm\omega}e^{i\omega r^*}, r\to\infty \tag{4}$$

For solving the homogeneous equation, we need to integrate the equation over a long distance starting from a purely ingoing pulse of radiation at the event horizon, and the coefficient $B^{\rm in}_{lm\omega}$ is not available numerically due to the presence of a long-ranged potential. Sasaki and Nakamura transformed the Teukolsky equation concerning $R_{lm\omega}$ to the Sasaki-Nakamura equation [21] concerning $X_{lm\omega}$. The potential of the Sasaki-Nakamura equation is short-ranged, so the equation can be computed numerically:

$$\frac{d^2X_{lm\omega}}{dr*^2} - F(r)\frac{dX_{lm\omega}}{dr*} - U(r)X_{lm\omega} = 0\,, \tag{5}$$

where $r*$ is the tortoise coordinate, $F(r)$ and $U(r)$ are the potentials of the Sasaki-Nakamura equation. The transform rlue from the Sasaki-Nakamura function to the Teukolsky function:

$$R_{lm\omega} = \frac{1}{\eta}\left[\left(\alpha + \frac{\beta_{,r}}{\Delta}\right)X_{lm\omega} - \frac{\beta}{\Delta}X_{lm\omega,r}\right] \tag{6}$$

the functions α, β, η and the potentials $F(r)$, $U(r)$ can be found in [22]. Note that the expression for η given in [22] is an expansion over $1/r$, which fails to recover reasonable results when r goes to the horizon (because η has to diverge as Δ^2 when $r\to r_+$). Original expression for η is given in Eq. (2.8c) of Sasaki-Nakamura's original article [21]:

$$\eta = \alpha\left(\alpha + \frac{d\beta/dr}{\Delta}\right) - \frac{\beta}{\Delta}\left(\frac{d\alpha}{dr} + \frac{\beta V(r)}{\Delta^2}\right) \tag{7}$$

The Sasaki-Nakamura equation admits two homogeneous solutions having purely sinuous asymptotic behavior due to the short ranges of potential $U(r)$:

$$X^H_{lm\omega} = A^{\rm hole}_{lm\omega}e^{-ipr*}, r\to r_+;\quad X^H_{lm\omega} = A^{\rm out}_{lm\omega}e^{i\omega r*} + A^{\rm in}_{lm\omega}e^{-i\omega r*},\quad r\to\infty \tag{8}$$

and

$$X^\infty_{lm\omega} = C^{\rm out}_{lm\omega}e^{ipr*} + C^{\rm in}_{lm\omega}e^{-ipr*}, r\to r_+;\quad X^\infty_{lm\omega} = C^\infty_{lm\omega}e^{i\omega r*}, r\to\infty, \tag{9}$$

where $p = \omega - ma/2Mr_+$. Now, an ECO has a reflecting boundary at r_0 where is very near the position of horizon r_+, i.e., $r_0 = r_+ + \epsilon$, and $\epsilon \ll 1$ [5]. Here, we assume r_0 is a constant. The solution reflected by the boundary is the combination of X^H and X^∞

$$X^{\rm ref}_{lm\omega} = \mathcal{K}X^\infty_{lm\omega} + X^H_{lm\omega} \tag{10}$$

which satisfies the reflecting boundary condition at the surface $r_0 = r_+ + \epsilon$ with reflectivity $\tilde{\mathcal{R}}$

$$X^{\rm ref} \propto e^{-ip(r*-r_0*)} + \tilde{\mathcal{R}}e^{ip(r*-r_0*)},\qquad r*\to r_0*\,. \tag{11}$$

Taking the asymptotic behavior of $X^{H,\infty}_{lm\omega}$ in Eq. (8, 9) into the above boundary condition, one can find $\mathcal{K}$:

$$\mathcal{K} = \frac{\tilde{\mathcal{R}} e^{-2ipr_0 *} \mathcal{T}_{BH}}{1 - \tilde{\mathcal{R}} e^{-2ipr_0 *} \mathcal{R}_{BH}} \quad \text{with} \quad \mathcal{T}_{BH} \equiv \frac{C^{\infty}}{C^{\text{out}}}, \; \mathcal{R}_{BH} \equiv \frac{C^{\text{in}}}{C^{\text{out}}}. \tag{12}$$

Finally, the GW waveform from a small object inspiraling an ECO is

$$\begin{aligned} & h_{+}^{\text{ECO}}(R,\theta,\phi,t) - i h_{\times}^{\text{ECO}}(R,\theta,\phi,t) \\ & = \frac{2}{R} \sum_{lm} \frac{1}{\omega^2} \left(Z^{H}_{lm\omega} + \mathcal{K} \frac{D^{\infty}_{lm\omega}}{B^{\text{hole}}_{lm\omega}} Z^{\infty}_{lm\omega} \right) {}_{-2}S^{a\omega}_{lm}(\theta) e^{i[m\phi - \omega_m (t - r*)]}. \end{aligned} \tag{13}$$

where $Z^{H,\infty}_{lm\omega}$ is given in Eq.(4.10) of [22]. The energy flux of gravitational radiation is decomposed by two parts $\dot{E} = \dot{E}^{\infty} + \dot{E}^{\text{H}}$ (here the dot means d/dt), i.e., the flux goes to the infinity and down to the horizon where the infinity flux is written as

$$\dot{E}^{\infty} = \sum_{l,m} \frac{|Z^{H}_{lm\omega} + \mathcal{K} \frac{D^{\infty}_{lm\omega}}{B^{\text{hole}}_{lm\omega}} Z^{\infty}_{lm\omega}|^2}{4\pi\omega^2}, \tag{14}$$

and the horizon one is

$$\dot{E}^{\text{H}} = \sum_{l,m} \alpha_{lm\omega} \frac{\left| \mathcal{T} Z^{\infty} \left(1 + \mathcal{K} \frac{D^{\text{in}}}{B^{\text{hole}}} \right) \right|^2}{4\pi\omega^2}. \tag{15}$$

Note the $\alpha_{lm\omega}$ here is not same as the α in the Eq. (7). The transmissivity $\mathcal{T}$ has a relation with reflection factor: $\mathcal{T}^2 + \tilde{\mathcal{R}}^2 = 1$. The relation between asymptotic amplitudes of Sasaki-Nakamura functions and Teukolsky functions [23]:

$$B^{\text{in}}_{lm\omega} = -\frac{1}{4\omega^2} A^{\text{in}}_{lm\omega}, \quad B^{\text{hole}}_{lm\omega} = -\frac{1}{d_{lm\omega}} A^{\text{hole}}_{lm\omega} \tag{16}$$

$$D^{\text{in}}_{lm\omega} = -\frac{1}{d_{lm\omega}} C^{\text{in}}_{lm\omega}, \quad D^{\infty}_{lm\omega} = -\frac{4\omega^2}{c_0} C^{\infty}_{lm\omega} \tag{17}$$

The coefficients c_0, $d_{lm\omega}$ and $\alpha_{lm\omega}$ can be found in [22]. Naturally, if we set $\tilde{\mathcal{R}} = 0$, all the results go back to the familiar equations of black holes.

3 Energy fluxes

Firstly, due to the existence of a hard surface, the total energy fluxes will be slightly different from the case of a black hole. How to calculate the energy fluxes is expressed in Eqs. (14, 15). If we choose $\mathcal{K} = 0$, i.e., $\tilde{\mathcal{R}} = 0$, then the energy fluxes will go back to the case of a black hole. The difference of total energy fluxes between ECO and BH cases depends on the orbital radius r or equivalent the orbital frequency ω_{orb}, reflectivity factor $\tilde{\mathcal{R}} = 0$, the location of the hard surface r_0 and also the spin of the central body a.

Figure 3 shows the relative differences of energy fluxes $\Delta\dot{E}/\dot{E}$ between ECO and BH when one changes the orbital frequency and the location of the ECO surface. We can see that $\Delta\dot{E}/\dot{E}$ have a clear power-law with the orbital frequency when the frequency is not large. This phenomenon has been revealed by the post-Newtonian approximation [24]. In the right panel of this figure, we can find that when $a = 0.3$, the difference in energy fluxes is almost zero, this is due to the orbital frequency being almost equal to the horizon frequency of the central body. This will be discussed later.

Now, let's see how the differences in energy fluxes vary with different spins. In Fig. 4, for different phases of reflectivity factors, the magnitude, and oscillation are different. Very interestingly, all the lines are gathered at zero for a special spin value. We find that at this spin value, the frequency of the BH horizon or the quantum surface of ECO equals the orbital frequency.

We can look at the details of how the energy fluxes vary with the phase of reflectivity factor, see Fig. 5. In this figure, each quadrant corresponds to a different boundary position (see the caption in Fig. 5 for details). Within each quadrant, the radius represents the absolute value of the reflectivity $\tilde{\mathcal{R}}$, and the angle reflects the ratio between the real part and imaginary one of $\tilde{\mathcal{R}}$. For example, if $\tilde{\mathcal{R}}$ only has a real part, then the angle with the horizontal line is 0, and if this angle is 90°, means the reflectivity only has imaginary part. So this angle is just the argument of $\tilde{\mathcal{R}} = |\tilde{\mathcal{R}}| e^{i\phi}$. These results indicate that not only the boundary position and magnitude of reflectivity but also the phase (argument) can influence the energy fluxes. In the following discussion, we always only take $\tilde{\mathcal{R}}$ as a real number.

Figure 6 shows the relative differences of energy fluxes $\Delta\dot{E}/\dot{E}$ between ECO and BH when one changes the reflectivity factor and orbital radii. We can clearly see that the magnitude of $\Delta\dot{E}/\dot{E}$ is at the order of 10^{-3}–10^{-2}. For comparable mass-ratio binaries, this error is too small to produce an observable effect in the LIGO band. However, if the mass ratio becomes smaller, for example down to 10^{-2}, this flux error should produce enough dephasing because of the much more cycles before the merger and may induce a failure of detection.

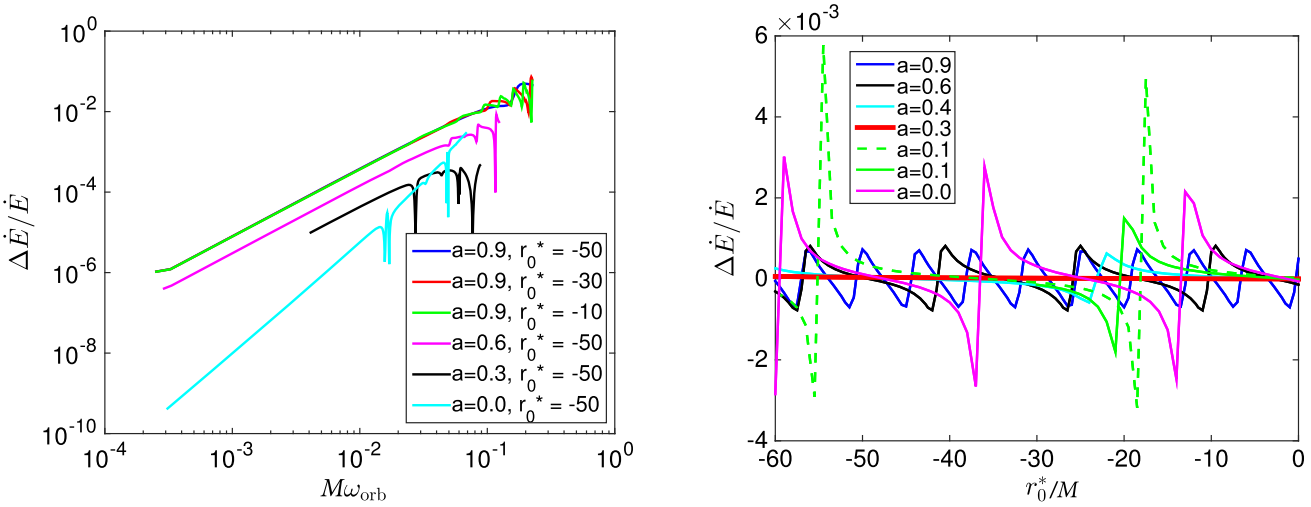

Fig. 3 Relative differences of energy fluxes $\Delta\dot{E}/\dot{E}$ between ECO and BH. Left panel: $\Delta\dot{E}/\dot{E}$ as a function with varied orbital frequency; right panel: $\Delta\dot{E}/\dot{E}$ as a function with a varied surface location and the orbital radii are fixed to r = 6 M for different spins

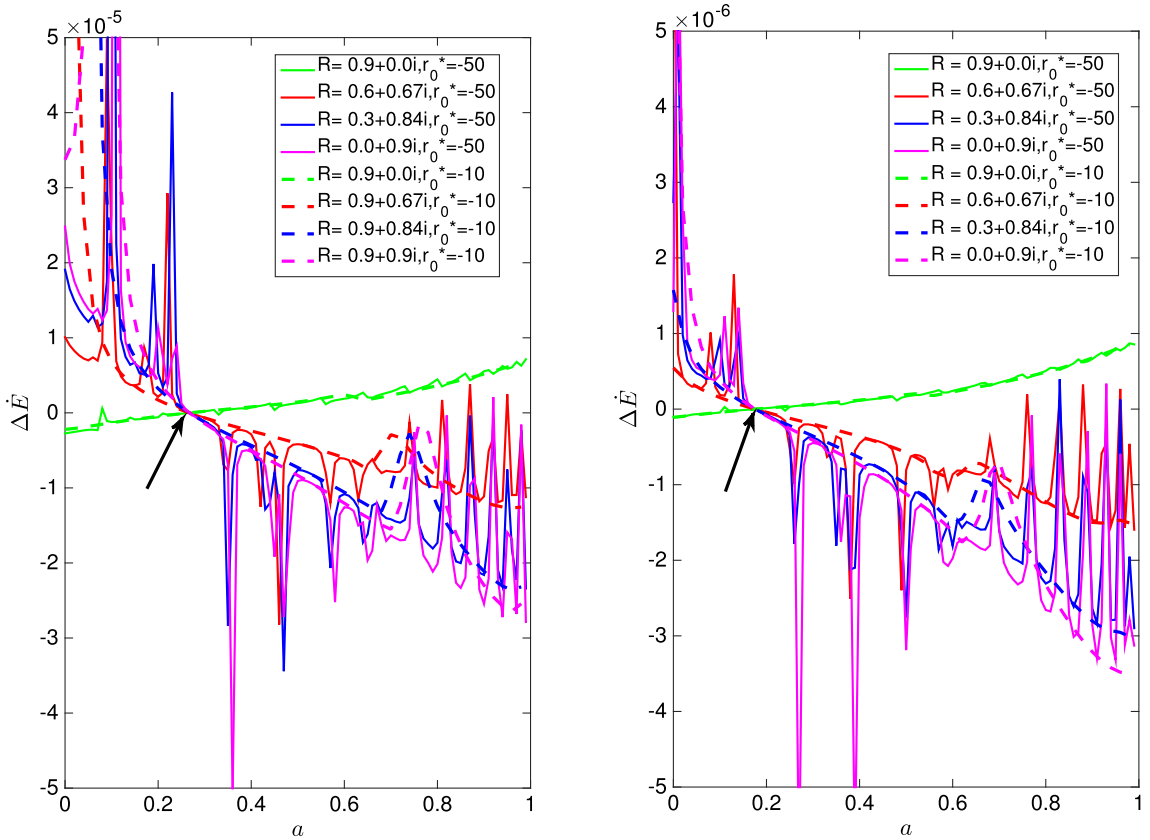

Fig. 4 The differences of energy fluxes $\Delta\dot{E}$ between ECO and BH. Left panel: $\Delta\dot{E}$ as a function versus spin with a varied phase of reflectivity factors, and the orbital frequency is fixed to the innermost-stable circular orbit (ISCO, $r = 6M$) one for nonspinning BH or ECO; right panel: The same with the left panel but the orbital frequency is fixed to the one with orbital radii $r = 8M$ for non-spinning BH or ECO

For investigating the effects on GWs from the hard surface of ECO, we use the energy fluxes (14,15) to evolve the orbits of EMRBs in Fig. 2 and generate the waveforms by Eq. (7). In the left panel of Fig. 7, the waveform from an NS inspiraling into an MBH and the one from an NS inspiraling into an ECO with $\tilde{\mathcal{R}} = 0.9$ are shown. One can see an obvious difference between the

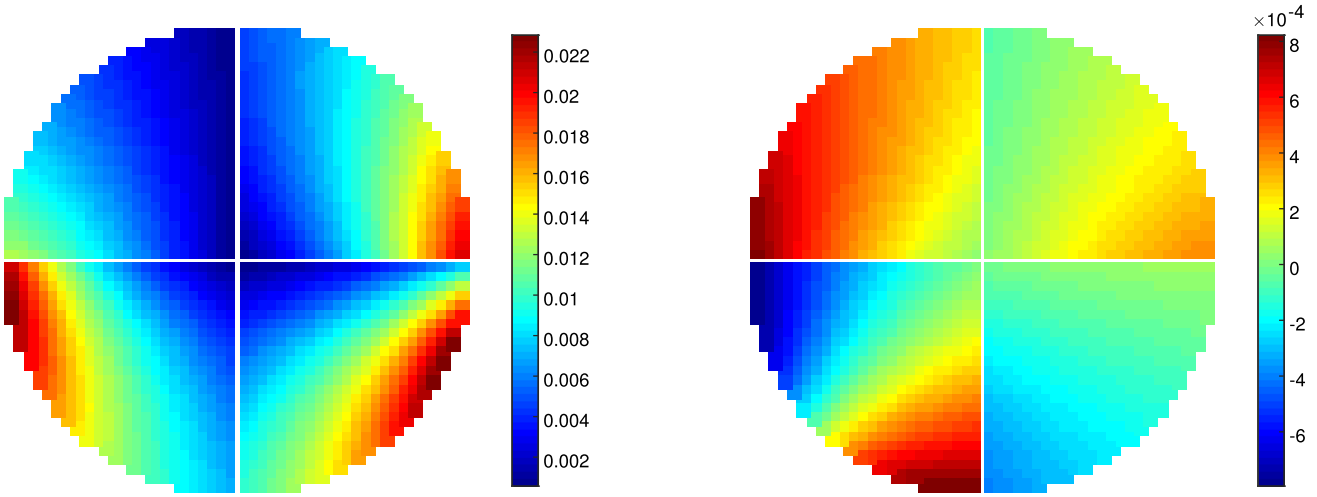

Fig. 5 Relative differences of energy fluxes $\Delta\dot{E}/\dot{E}$ between ECO and BH. Left panel: $\Delta\dot{E}$ of a small object orbiting at radii 3 M around a BH or ECO with spin 0.9 as a function versus varied phase of reflectivity factors, the location of ECO surface are -50, -30, -20 and -10 from top-right panel to bottom-right panel counterclockwise; right panel: The same with the left panel but the orbital radii $r = 6M$

two waveforms. By using matched filtering technology, we can quantitatively give out the difference of two waveforms ($h_a(t)$ and $h_b(t)$), i.e., mismatch.

$$\text{mismatch} \equiv 1 - \max_{t_c,\phi_c}\left(\frac{< h_a|h_b >}{\sqrt{< h_a|h_a >< h_b|h_b >}}\right), \tag{18}$$

where $< h_a|h_b >$ is the standard matched-filtering inner product between two waveforms and t_c (ϕ_c) is the time (phase) of coalescence,

$$< h_a|h_b > \equiv 2\int_0^\infty df\,\frac{\tilde{h}_a^*(f)\tilde{h}_b(f) + \tilde{h}_a(f)\tilde{h}_b^*(f)}{S_n(f)}, \tag{19}$$

where $\tilde{h}$ means the frequency-domain waveform and $*$ the complex conjugate. In the following analysis, the noise power spectral density $S_n(f)$ is taken from the LIGO noise, here we use the updated advanced LIGO sensitivity design curve LIGO-T1800044. In the right panel of Fig. 7, a mismatch of waveforms from BH and ECO with varied $\tilde{\mathcal{R}}$ are shown. It demonstrates that once $\tilde{\mathcal{R}} > 0.5$, the hard surface of ECO will induce a considerable mismatch on the waveforms and in principle can be detected from the GW data.

However, one may suspect that the effect of a hard surface on the energy fluxes can be mimicked by other physical parameters. The mass-ratio and spin a can also change the energy fluxes and then the orbital evolution and waveforms. It means that the reflectivity is possibly degenerate with other parameters and then cannot be recognized from the GW data. For checking this point, we match the waveform of an EMRB 1.5 $M_\odot$ NS + 60 $M_\odot$ ECO with $\tilde{\mathcal{R}} = 0.9$ and $a = 0.6$, and a group of EMRBs with mass-ratio from 0.01 to 0.04 and spin of BH from 0.5 to 0.7. In Fig. 8, the match results show that the best match is the BH chooses the same spin and mass-ratio of ECO. The best match is still less than 0.9, and for different spin and mass-ratio cases, one cannot find a waveform from BH that can mimic the one from ECO. This may prove that the degeneracy of $\tilde{\mathcal{R}}$ does not exist. In other words, if the compact object is an ECO, we can recognize it from BH and find the no-horizon extremely compact object.

Furthermore, for estimating the measurement accuracy of the reflectivity factor and surface location by the EMRB signals, we employ the Fisher matrix to do the parameter estimation. We use waveforms with the signal-to-noise ratio (SNR) is about 130. The Fisher information matrix for a GW signal h parameterized by λ is given by [25]

$$\Gamma_{ij} = \left\langle \frac{\partial h}{\partial \lambda_i} | \frac{\partial h}{\partial \lambda_j} \right\rangle, \tag{20}$$

where λ is the waveform parameters including $\mathcal{R}$ and r_0*. In the case of high SNR, the errors of parameters can be approximated as the square root of the diagonal elements of the inverse of Γ_{ij}, i.e., $\Delta\lambda_i \approx \sqrt{(\Gamma^{-1})_{ii}}$. We find that the reflectivity factor and surface location can be measured to about $\Delta\lambda_i/\lambda_i \sim 1.3\%$ and 1.5%, respectively. The corresponding likelihood is $\mathcal{L}(\lambda) \propto e^{-\frac{1}{2}\Gamma_{ij}\Delta\lambda_i\Delta\lambda_j}$ [25, 26] and is shown in Fig. 9. These results demonstrate that once LIGO can catch EMRB events, without observing the echo signals, just from the inspiraling waveforms, one can constrain the properties of the surface of BHs with a positive accuracy.

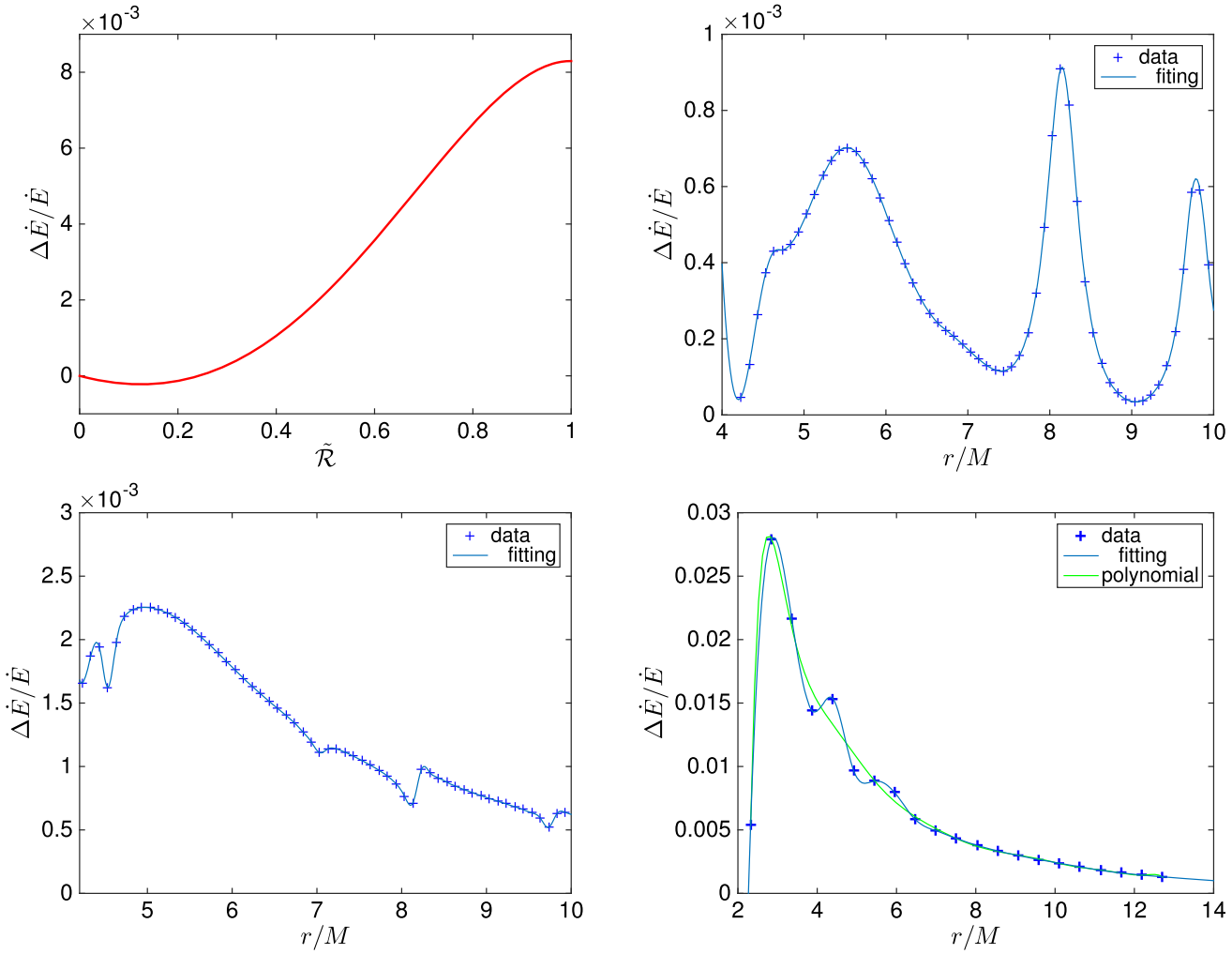

Fig. 6 Relative differences of energy fluxes $\Delta\dot{E}/\dot{E}$ between ECO and BH. Top-left panel: $\Delta\dot{E}/\dot{E}$ as a function with varied reflectivity $\tilde{\mathcal{R}}$ when $a = 0.9$, $r_0^* = -50$ and $r = 6M$; top-right panel: $\Delta\dot{E}/\dot{E}$ as a function with varied orbital radii when $a = 0.5$, $r_0^* = -50$ and $\tilde{\mathcal{R}} = 0.5$; bottom panels: The same with the top-right one but $\tilde{\mathcal{R}} = 0.9$, $a = 0.5$ and 0.9 for left and right one, respectively

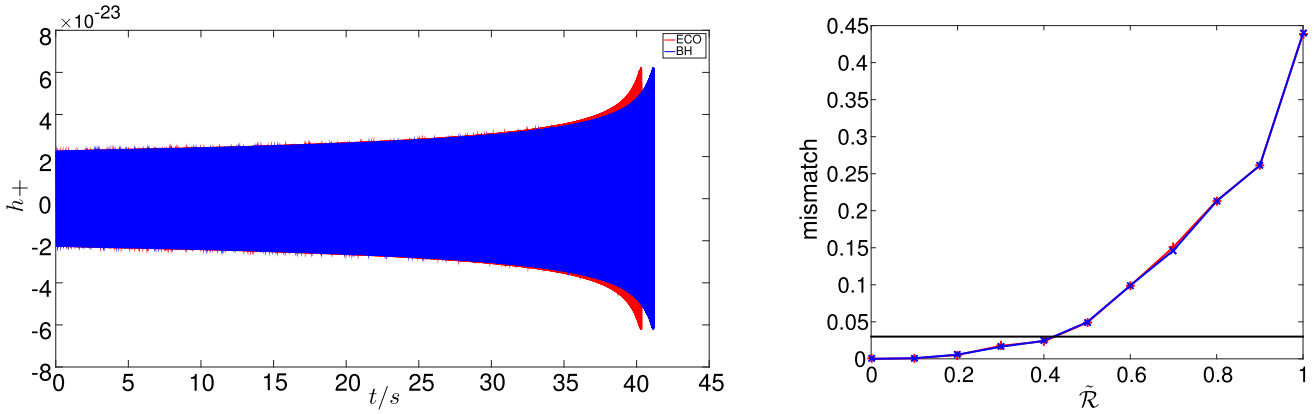

Fig. 7 Left panel: gravitational waves of MBH and ECO's EMRBs. The mass of the massive compact body (ECO or BH) is 140 $M_\odot$ and the small object is 1.4 $M_\odot$, the spin of the massive body is 0.9, reflectivity is 0.9 and surface location $r_0^* = -50$. Right panel: mismatch results of the two kinds of waveforms while the reflectivity $\tilde{\mathcal{R}}$ of the hard surface of ECO from 0 to 1

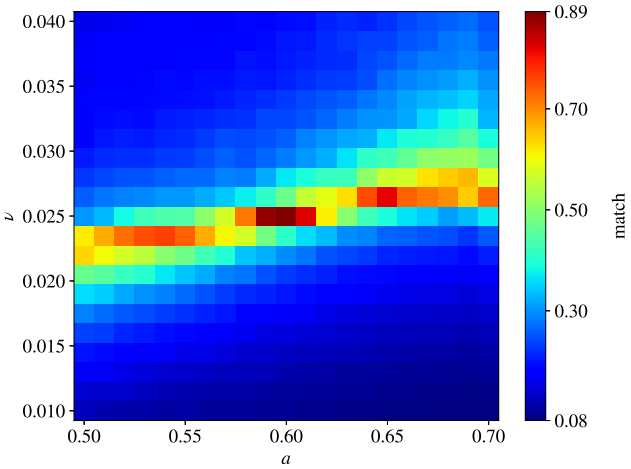

Fig. 8 Match results between ECO waveforms and a group of BH waveforms with varied mass ratio ν and spin a

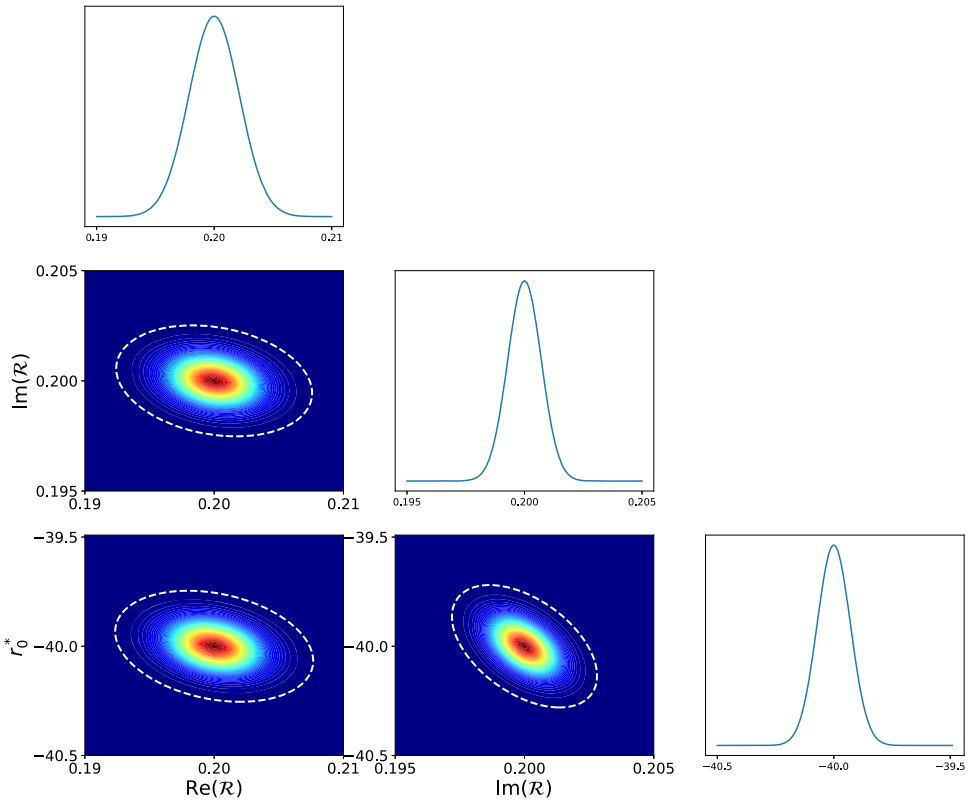

Fig. 9 Likelihood of $\mathcal{R}$ and r_0^* which are derived from the Fisher matrix. The white dashed ellipse is shown at 3σ

4 Conclusions

The nature of the extremely compact object is quite important in theoretical physics. Though black holes are very popular, the other candidates like the firewall model are still living [5]. Due to the hard surface at the Plank scale near the corresponding position of the BH horizon, there are a lot of predictions of GW echoes after the ringdown in the literature. In 2017, Abedi et al. claimed that they had found tentative evidence of echoes at a combined 2.9σ significance level [27]. However, their result was questioned [28, 29]. Various teams have also proposed methods to estimate the parameters of the gravitational-wave echoes and to search for echoes [11–15, 30, 31]. Until now, there are no more reports about finding echo signals.

In the present paper, we do not consider the direct echo signals; alternatively, we try to reveal the effect of the quantum surface at the Planck scale outside of the horizon in the inspiraling stage of binary merger. Due to the existence of a quantum surface, the energy fluxes and gravitational waveform are both modified. However, this modification is usually too small to be recognized in the GW data from comparable mass-ratio binaries. Fortunately, if the mass ratio is smaller than 1:10, thanks to the longer inspiral, this modification due to the possible hard surface may be extracted from the GW data. In the future, we expect to do some data analysis for LVK events.

By modifying the boundary condition of the Teukolsky equation, we numerically calculate the orbital evolution and waveforms from a compact object (NS, BH, PBH) inspiraling a massive ECO. Our calculation shows that if the hard surface exists and its reflectivity factor is large enough ($>\approx 0.5$), by matched-filtering technology, we may have a chance to study the nature of extremely compact objects and answer if they are black holes or ECOs.

Acknowledgements This work is supported by The National Key R &D Program of China (No. 2021YFC2203002), NSFC No. 11773059 and No. 12173071, and the Strategic Priority Research Program of the CAS under Grants No. XDA15021102. W. H. is supported by CAS Project for Young Scientists in Basic Research YSBR-006. We thank Yanbei Chen, Shuo Xin, and Ling Sun for very useful discussions.

Data availability The data underlying this article will be shared on reasonable request to the corresponding author Wen-Biao Han.

References

1. B.P. Abbott et al., GWTC-1: A gravitational-wave transient catalog of compact binary mergers observed by LIGO and Virgo during the first and second observing runs. Phys. Rev. X **9**(3), 031040 (2019)
2. N.V. Krishnendu, K.G. Arun, C.K. Mishra, Testing the binary black hole nature of a compact binary coalescence. Phys. Rev. Lett. **119**(9), 091101 (2017)
3. R. Abbott, et al., Tests of General Relativity with GWTC-3. arXiv e-prints arXiv:2112.06861 (2021)
4. R. Carballo-Rubio, F. Di Filippo, S. Liberati, M. Visser, Phenomenological aspects of black holes beyond general relativity. Phys. Rev. D **98**(12), 124009 (2018)
5. V. Cardoso, P. Pani, Testing the nature of dark compact objects: a status report. Living Rev. Relat. **22**(1), 4 (2019)
6. V. Cardoso, P. Pani, Tests for the existence of black holes through gravitational wave echoes. Nat. Astro. **1**, 586–591 (2017)
7. Z. Mark, A. Zimmerman, S.M. Du, Y. Chen, A recipe for echoes from exotic compact objects. Phys. Rev. D **96**(8), 084002 (2017)
8. S.M. Du, Y. Chen, Searching for near-horizon quantum structures in the binary black-hole stochastic gravitational-wave background. Phys. Rev. Lett. **121**(5), 051105 (2018)
9. B. Chen, Y. Chen, Y. Ma, K.L.R. Lo, L. Sun, Instability of exotic compact objects and its implications for gravitational-wave echoes. arXiv e-prints arXiv:1902.08180 (2019)
10. S. Xin, B. Chen, R.K.L. Lo, L. Sun, W.B. Han, X. Zhong, M. Srivastava, S. Ma, Q. Wang, Y. Chen, Gravitational-wave echoes from spinning exotic compact objects: numerical waveforms from the Teukolsky equation. Phys. Rev. D **104**(10), 104005 (2021)
11. A. Maselli, S.H. Völkel, K.D. Kokkotas, Parameter estimation of gravitational wave echoes from exotic compact objects. Phys. Rev. D **96**(6), 064045 (2017)
12. K.W. Tsang, M. Rollier, A. Ghosh, A. Samajdar, M. Agathos, K. Chatziioannou, V. Cardoso, G. Khanna, C. Van Den Broeck, A morphology-independent data analysis method for detecting and characterizing gravitational wave echoes. Phys. Rev. D **98**(2), 024023 (2018)
13. A.B. Nielsen, C.D. Capano, O. Birnholtz, J. Westerweck, Parameter estimation and statistical significance of echoes following black hole signals in the first Advanced LIGO observing run. Phys. Rev. D **99**(10), 104012 (2019)
14. R.K.L. Lo, T.G.F. Li, A.J. Weinstein, Template-based gravitational-wave echoes search using Bayesian model selection. Phys. Rev. D **99**(8), 084052 (2019)
15. N. Uchikata, H. Nakano, T. Narikawa, N. Sago, H. Tagoshi, T. Tanaka, Searching for black hole echoes from the LIGO-Virgo catalog GWTC-1. Phys. Rev. D **100**(6), 062006 (2019)
16. S. Datta, R. Brito, S. Bose, P. Pani, S.A. Hughes, Tidal heating as a discriminator for horizons in extreme mass ratio inspirals. Phys. Rev. D **101**, 044004 (2020)
17. R. Abbott, et al., GWTC-3: Compact Binary Coalescences Observed by LIGO and Virgo During the Second Part of the Third Observing Run. arXiv e-prints arXiv:2111.03606 (2021)
18. S.A. Teukolsky, Perturbations of a rotating black hole. I. Fundamental Equations for Gravitational, Electromagnetic, and Neutrino-Field Perturbations. ApJ, **185**, 635–648 (1973)
19. S. Bernuzzi, A. Nagar, Binary black hole merger in the extreme-mass-ratio limit: a multipolar analysis. Phys. Rev. D **81**(8), 084056 (2010)
20. W.B. Han, Z. Cao, Constructing effective one-body dynamics with numerical energy flux for intermediate-mass-ratio inspirals. Phys. Rev. D **84**(4), 044014 (2011)
21. M. Sasaki, T. Nakamura, Gravitational radiation from a Kerr Black Hole. I Formulation and a Method for Numerical Analysis. Progress of Theoretical Physics **67**(6), 1788–1809 (1982)
22. S.A. Hughes, Evolution of circular, nonequatorial orbits of Kerr black holes due to gravitational-wave emission. Phys. Rev. D **61**(8), 084004 (2000)
23. Y. Mino, M. Sasaki, M. Shibata, H. Tagoshi, T. Tanaka, Chapter 1 Black hole perturbation. Prog. Theor. Phys. Suppl. **128**, 1–121 (1997)
24. P.M. Sá, A.B. Henriques, Parametric resonance and cosmological gravitational waves. Phys. Rev. D **77**(6), 064002 (2008)
25. C. Cutler, É.E. Flanagan, Gravitational waves from merging compact binaries: How accurately can one extract the binary's parameters from the inspiral waveform? Phys. Rev. D **49**(6), 2658–2697 (1994)
26. S. Babak, J. Gair, A. Sesana, E. Barausse, C.F. Sopuerta, C.P.L. Berry, E. Berti, P. Amaro-Seoane, A. Petiteau, A. Klein, Science with the space-based interferometer LISA. V. Extreme mass-ratio inspirals. Phys. Rev. D **95**(10), 103012 (2017)
27. J. Abedi, H. Dykaar, N. Afshordi, Echoes from the abyss: tentative evidence for Planck-scale structure at black hole horizons. Phys. Rev. D **96**(8), 082004 (2017)
28. G. Ashton, O. Birnholtz, M. Cabero, C. Capano, T. Dent, B. Krishnan, G.D. Meadors, A.B. Nielsen, A. Nitz, J. Westerweck, Comments on: "Echoes from the abyss: Evidence for Planck-scale structure at black hole horizons". arXiv e-prints arXiv:1612.05625 (2016)
29. J. Abedi, H. Dykaar, N. Afshordi, Echoes from the Abyss: The Holiday Edition! arXiv e-prints arXiv:1701.03485 (2017)
30. J. Westerweck, A.B. Nielsen, O. Fischer-Birnholtz, M. Cabero, C. Capano, T. Dent, B. Krishnan, G. Meadors, A.H. Nitz, Low significance of evidence for black hole echoes in gravitational wave data. Phys. Rev. D **97**(12), 124037 (2018)
31. R.S. Conklin, B. Holdom, J. Ren, Gravitational wave echoes through new windows. Phys. Rev. D **98**(4), 044021 (2018)